Science of the Total Environment 650 (2019) 796–808

Contents lists available at ScienceDirect

Science of the Total Environment

journal homepage: www.elsevier.com/locate/scitotenv

Characterizing the atmospheric conditions during the 2010 heatwave in Rio de Janeiro marked by excessive mortality rates

João L. Geirinhas [a,*], Ricardo M. Trigo [a], Renata Libonati [b,e], Lucas C.O. Castro [b], Pedro M. Sousa [a], Caio A.S. Coelho [c], Leonardo F. Peres [b,f], Mônica de Avelar F.M. Magalhães [d]

[a] Instituto Dom Luiz, Faculdade de Ciências da Universidade de Lisboa, Campo Grande, Lisboa, Portugal
[b] Departamento de Meteorologia, Universidade Federal do Rio de Janeiro (UFRJ), Rio de Janeiro, Brazil
[c] Centro de Previsão de Tempo e Estudos Climáticos (CPTEC), Instituto Nacional de Pesquisas Espaciais (INPE), Cachoeira Paulista, SP, Brazil
[d] Instituto de Comunicação e Informação Científica e Tecnológica em Saúde (ICICT), Fundação Oswaldo Cruz (FIOCRUZ), Rio de Janeiro, Brazil
[e] Centro de Estudos Florestais, Instituto Superior de Agronomia, Universidade de Lisboa, Lisboa, Portugal
[f] Instituto Português do Mar e da Atmosfera (IPMA), Lisboa, Portugal

HIGHLIGHTS

- A total of 3006 deaths was recorded representing an excess of 737 deaths.
- Higher mortality risk for women compared to men and particularly for the elderly
- Quasi-stationary mid-atmospheric anticyclonic anomaly over the South Atlantic
- Relevant soil-atmosphere feedback mechanisms for the Heat Wave development
- Regional katabatic winds were responsible for heating the already warm air mass.

GRAPHICAL ABSTRACT

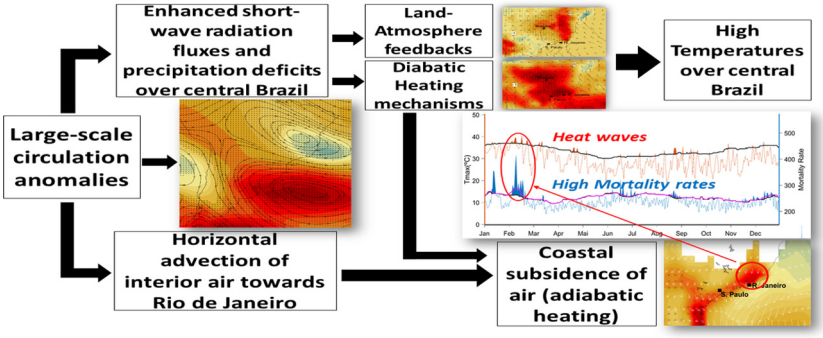

ARTICLE INFO

Article history:
Received 20 June 2018
Received in revised form 4 September 2018
Accepted 4 September 2018
Available online 5 September 2018

Editor: SCOTT SHERIDAN

Keywords:
Climate extremes
Brazil
Human impacts
Circulation patterns

ABSTRACT

Global temperatures have increased considerably over the last decades, directly impacting the number, intensity and duration of extreme events such as heat waves. Climate model projections accounting for anthropogenic factors indicate that deadly mega-heat waves are likely to become more frequent in the future. Although the atmospheric features and social-economic related impacts of heat waves have already been documented in various regions around the world, for other highly populated regions, such as the Metropolitan Region of Rio de Janeiro (MRRJ), a similar objective assessment is still needed. Heat waves directly impact the public health sector and particularly the less wealthy and elderly population groups. During February 2010, an elevated mortality peak occurred during a 8-day period (from 2 to 9 Feb 2010) characterized as a heat wave episode in MRRJ. A total excess of 737 deaths was recorded with the elderly group registering the highest mortality incidence. During this heat wave period, a quasi-stationary anticyclonic anomaly forced in altitude by a Rossby wave train was established over the south Brazilian coast. At the surface, the meteorological scenario from January 2010 to the heat wave period was marked by clear sky conditions, large precipitation deficits, and enhanced diabatic heating. During the heat wave period, warm and dry air masses were advected from interior regions towards the MRRJ, exacerbating temperature conditions by

* Corresponding author at: Centro de Geofísica da Universidade de Lisboa, Laboratório Associado IDL (Instituto Dom Luiz), Faculdade de Ciências da Universidade de Lisboa, Campo Grande, Edifício C8, Piso 3, 1749-016 Lisboa, Portugal.
E-mail address: jlgeirinhas@fc.ul.pt (J.L. Geirinhas).

https://doi.org/10.1016/j.scitotenv.2018.09.060

pronounced subsidence and adiabatic heating mechanisms. All these conditions contributed to pronounced positive temperature anomalies, reinforced by land-atmosphere feedbacks.

1. Introduction

The pervasive positive temperature trend in various parts of the world has become a high-priority issue for today's society, generating growing concern about current and future impacts of associated extremes events such as droughts, floods, storms, heat and cold waves (IPCC, 2012). The beginning of the 21st century in agreement with the previous 1990s and 1980s decades of the 20th century, have been characterized by a continuous rise in the global mean temperature with 17 out of the 18 warmest years on record all occurring in the beginning of the 21st century (IPCC, 2014; NOAA, 2018). Moreover, temperature extremes, such as heat waves (HWs) have been continuously showing increasing trends regarding frequency, intensity, and duration (Seneviratne et al., 2014). As a consequence, during the last years, a new HW class was identified, the so-called mega HWs characterized by historical record events regarding the spatial extent, duration, intensity and the severity of their impacts on ecosystems and society (Barriopedro et al., 2011; Miralles et al., 2014). Examples of these mega HWs are the 2003 and 2017 European HWs, as well as the 2010 Russian and the 2011 US (Texas) HWs (Qian et al., 2016).

HWs are known to impinge a wide range of impacts in public health (Gasparrini and Armstrong, 2012), in several socio-economic sectors (Garcia-Herrera et al., 2010; Linares and Díaz, 2008), in ecosystem's water availability and in vegetation/animal stress levels including vegetation fires (Bastos et al., 2014; Gusso et al., 2014). Extremely hot temperatures are capable of perturbing the human biological mechanisms, especially those related to thermoregulatory body response, which might, in turn, aggravate some diseases, particularly cardiovascular and respiratory conditions (Braga et al., 2002; Hajat et al., 2005). Recent studies have established a relationship between mortality and several environmental variables, especially temperature (Gasparrini et al., 2015; Gasparrini and Armstrong, 2012; McMichael et al., 2008; Son et al., 2016). The heat effects are felt with more intensity by some population sectors, the so-called risk groups, such as elderly people and fragile individuals with chronic illnesses or pre-existing heart and respiratory diseases (Basu and Samet, 2002; Barnett, 2007; Bell et al., 2008; Trigo et al., 2009; Åström et al., 2011). Several studies have reported excess mortality rates during HW events primarily in the U.S.A., Australia, and Europe. For instance, at least 40.000 deaths were reported when extremely high temperatures were recorded during the 2003 European mega HW (Garcia-Herrera et al., 2010; Robine et al., 2008). In contrast, there are fewer studies evaluating the impact of HWs in mortality over South-America, although Muggeo and Hajat (2009) and Bell et al. (2008) observed an increase in non-accidental mortality among the elderly due to persistently warmer days. Gouveia et al. (2003) and Son et al. (2016) also reported an association between high temperatures in São Paulo and excess mortality rates, mainly due to respiratory diseases.

In South America, and particularly in Brazil, an increase in the frequency and intensity of extreme heat events has also been observed since the second half of the twentieth century (Bitencourt et al., 2016; Ceccherini et al., 2016; Cerne and Vera, 2011; Geirinhas et al., 2017; Hannart et al., 2015; Renom et al., 2011; Rusticucci, 2012; Rusticucci et al., 2017, 2016). For instance, extremely hot and dry conditions over southeastern Brazil (SEB) during the 2001 and 2014 summers led to a severe water resources crisis and important electricity production deficits (Herring et al., 2015; Coelho et al., 2016), a scenario that imposed constraints on the population for reaching thermal body comfort. In addition to the severe water supply crisis, the 2014 event triggered a dramatic increase in the number of forest fires in the region (Rodrigues et al., 2018).

Hot and dry summer events over the southeast region of Brazil have been associated to persistent anticyclonic patterns over the South Atlantic, near the south and southeast coasts of Brazil (Coelho et al., 2016; Grimm, 2003). This large-scale anticyclonic configuration is often related to an upper-level atmospheric wave-type flow and Rossby wave trains. Such wave trains induce a large-scale teleconnection between the Southeast Pacific, South America, and the South Atlantic Ocean, the so-called Pacific – South American Modes (Irving and Simmonds, 2016; Mo and Paegle, 2001; Renwick and Revell, 1999). The year of 2010 was also exceptionally hot and dry over all South America, being characterized by the occurrence of a large number of HW events in many Brazilian cities, namely São Paulo, Manaus, Recife and Brasília (Geirinhas et al., 2017). Moreover, during the 2009–2010 hydrological year the Amazon region experienced a historical drought, in association with a significant and prolonged precipitation deficit coupled to both high-temperature values and evaporation rates (Lewis et al., 2011; Marengo et al., 2011; Panisset et al., 2018). Such anomalous conditions have been linked to the manifestation of an El Niño event with anomalously warm sea surface temperatures (SST) in the central and eastern Pacific, and also to anomalously warm SST over the tropical North Atlantic Ocean (Coelho et al., 2012; Marengo and Espinoza, 2016).

Despite the role played by the El Niño event and the anomalously warm tropical North Atlantic, it is important to note that these extreme climatic events occurred within the context of positive temperature trends (regarding both Tmax and Tmin values) recorded since 1960 over South America and Brazil (Marengo and Camargo, 2008; de Barros Soares et al., 2017). The atmospheric mechanisms contributing to the manifestation of northern hemisphere HW events, such as the European 2003 and the Russian 2010 mega HWs, have been well identified and characterized (e.g., Trigo et al., 2005; Fischer et al., 2007; Garcia-Herrera et al., 2010; Fischer, 2014; Qian et al., 2016; Tomczyk, 2017). However, for South America, relatively fewer studies have explored the main large-scale and regional atmospheric circulation mechanisms during the preceding weeks/months and the HW period itself.

One of the most intense and prolonged HW affecting the Metropolitan Region of Rio de Janeiro (MRRJ), a major population center in Brazil, was recorded at the beginning of 2010, during the week spanning from 2 and 9 February 2010. This event was characterized by daily maximum temperatures (Tmax) higher than the calendar day climatological Tmax 90th percentile for eight consecutive days. According to the local and national media, this period was defined as an extremely hot episode associated to abnormally high mortality. Besides the early February 2010 HW event, the city of Rio de Janeiro recorded several other periods of consecutive days with abnormally high-temperature values. However, to the best of our knowledge, the 2010 HW event has never been properly assessed, neither from the meteorological perspective nor from the excessive mortality induced. By combining the knowledge produced when characterizing the atmospheric circulation conditions that prevailed during the manifestation of the observed HWs, with the proper use of weather and climate forecast models, which are designed to anticipate the occurrence of these conditions, it is becoming possible to predict the occurrence and the intensity of HWs. This knowledge and predictions are of extreme importance for preventing society and health services from potential mortality risk periods, particularly in densely populated areas. In fact, due to the so-called urban heat island effect and considering the projected increase in surface temperatures for the next decades (IPCC, 2014), people living in the metropolitan regions

of large cities such as MRRJ will be the ones being mostly affected by temperature extremes (Dereczynski et al., 2013; Lucena et al., 2013; Peres et al., 2018).

This paper aims to contribute to this theme, taking as its main objective the characterization of the atmospheric conditions observed during a severe mortality rate period in the MRRJ, identified as a HW period (2–9 February 2010), and then to establish a bridge between the observed abnormal high temperatures and this excessive mortality peak. A detailed characterization of the large-scale and regional atmospheric setting that contributed to the development and maintenance of this extremely hot event will be exposed and discussed.

2. Data and methodology

2.1. Mortality and temperature data for Rio de Janeiro

Daily mortality among residents for all-natural death causes (non-accidental or non-violent) for the metropolitan region of Rio de Janeiro (MRRJ) were obtained from death certificates of the Brazilian Health System database (DATASUS). This database is made available through the Data Science Platform developed by the Institute of Scientific and Technological Information in Health of the Oswaldo Cruz Foundation. The MRRJ mortality records for the 2000–2015 period were aggregated by age group (0–14; 15–29; 30–59; ≥60 years old) and gender. Following a similar methodology used in previous studies (Trigo et al., 2009), mortality values for the period 2–11 February 2010 were computed using the averaged period proportional mortality ratio methodology (APPMR):

$$\mathrm{APPMR}_i = \frac{\mathrm{M_i}}{(\mathrm{M_1} + \mathrm{M_2} + \cdots + \mathrm{M_{i-1}} + \mathrm{M_{i+1}} + \ldots + \mathrm{M_k})/(\mathrm{k}-1)} \quad (1)$$

with M the mortality observed in specific time periods and K the total number of years considered. A more intuitive interpretation of the APPMR index considers its values as the ratio between the observed mortality (O) and the expected mortality (E) during a specific time period. Hereafter APPMR will be referred to as the ratio "O/E". The excess mortality index defined as the difference between the observed and expected mortality levels, was another metric used to analyze the mortality data. Values of both excess mortality index and O/E ratio were computed for each age group and both genders.

The identification of the period from 2 to 9 February 2010 as a HW was performed using observed daily values of maximum surface air temperature (T_{max}) and applying a methodology successfully used in recent studies (Geirinhas et al., 2017; Perkins and Alexander, 2013). A HW is here defined as a period of three or more consecutive days characterized by daily T_{max} values above the climatological (1961–2014 base period) calendar day 90th T_{max} percentile calculated on a 15-day window (centered on the day in question). Such methodology is given by the CTX90pct index (Perkins and Alexander, 2013), a relative threshold (percentile-based) index that is an effective alternative to indices based on absolute thresholds (ex: ETCCDI indices – SU and TR). Absolute indices are not suitable on some regions because they don't consider seasonal and spatial variability (Perkins, 2011). Similar relative threshold indices were already successfully applied in previous studies of this kind for South America (Rusticucci et al., 2016; Bitencourt et al., 2016; Geirinhas et al., 2017). Many HW indices also consider Tmin values, and some of them even consider the joined effect of Tmin, Tmax and humidity values on thermal sensitivity. In our particular case we choose not to conduct our analysis based on Tmin values because they don't shown an effective relationship with mortality rates such as the one verified with Tmax. The temperature data was obtained from the Galeão meteorological station located in the international airport within the MRRJ (28.8°S, 43.28°W) and available from the ICEA network (Brazilian Air Traffic Control Institute).

2.2. Large-scale meteorological data

The large-scale and regional atmospheric mechanisms contributing to the manifestation of the investigated HW event were characterized through the analysis of anomaly composites (mean field removed). The HW composite for a specific meteorological parameter is defined as the mean of its observed values during the HW period. The data used to build these composites is derived from the ERA-Interim Reanalysis (Dee et al., 2011) fields from the European Centre for Medium-Range Weather Forecast (ECMWF). The data were collected for the period spanning from 1979 to 2014 and for the area limited by the following latitude and longitude ranges: 20°N–65°S and 140°W–26°W. It's important to note that the reanalysis period (1979–2014) is shorter than the longer period with station data (1961–2014), which was used to compute local Tmax/Tmin percentiles and to define the 2–9 February 2010 period as a HW. Large-scale data prior to 1979 for the southern hemisphere is dominated by missing values. The ERA-I reanalysis datasets start in 1979 as they rely extensively in data retrieved from satellites, which at that time, were crucial to provide a complete picture of climate variability and day-to-day meteorological conditions over the southern hemisphere (Ji et al., 2015). The main reason to stop the analysis in 2014 is simply related to the availability of Tmax and Tmin values from the main station of Galeão Airport ending in 2014.

The meteorological variables used in these anomaly composite fields are daily time series of sea level pressure (SLP), 500 and 250 hPa Geopotential height (H500, H250 respectively), 250 hPa meridional wind component (V250), 500 hPa and 250 hPa level temperature (T500, T250 respectively), maximum air temperature 2 m above the surface (Tmax), zonal and meridional wind components 10 m above the surface (u10, v10 respectively), relative air humidity at surface (RHsfc), total precipitation (Prec), surface net solar radiation (SRad), soil water content (SoilW) and surface sensible heat flux (SH). All values correspond to daily mean averages, except for Tmax, SRad, and SH. The daily maximum temperature values corresponding to the maximum temperature recorded on each day. Surface net solar radiation (SRad) and SH values correspond to 12h accumulated radiation fluxes (12 h–00 h). The soil water content corresponds to Layer 1, which is defined by ERA-Interim as a soil layer with a thickness of 0.7 m from the surface. The reanalysis data is based on observed measures in situ, however, it depends also on the quality of the forecast model used. The precipitation variable is mainly dependent on the forecast model used, and so its values are more susceptible to model systematic errors. Anomaly composites (mean field removed), as the ones used on this paper, filter considerably the impact of model biases (Trigo et al., 2004,) minimizing some of the inherent model errors.

To evaluate different mechanisms involved in the triggering and maintenance of the HW, we assessed the atmospheric circulation patterns identified in the anomaly composite fields recorded during the HW period. Here we adopt a similar approach to previous studies to diagnose in detail the main physical processes (horizontal advection, vertical advection, and diabatic processes) contributing to the increment in surface temperature (e.g., Sousa et al., 2018). Thus, for each grid point with temperature anomalies higher than 1 °C, we identified which process contributed more pronouncedly to the development of abnormal surface heating. Horizontal and vertical temperature advection were explicitly calculated by Eqs. (2) and (3), respectively:

$$\left(\frac{\Delta T}{\Delta t}\right)_h (\lambda, \phi, t) = -\vec{v}.\nabla_p T \quad (2)$$

$$\left(\frac{\Delta T}{\Delta t}\right)_v (\lambda, \phi, t) = -\omega \frac{T}{\theta}\frac{\partial \theta}{\partial p} \quad (3)$$

where $(\frac{\Delta T}{\Delta t})_h$ is the temperature advection by the horizontal wind, $(\frac{\Delta T}{\Delta t})_v$ is the temperature advection by the vertical motion, with (λ, ϕ, t) representing latitude, longitude and time, respectively, v is the

horizontal wind, T is the temperature, ω is the vertical velocity (p coordinates) and θ is the potential temperature. The temperature change rate due to diabatic processes was estimated as a residual from the previous two terms and using the temperature tendency equation:

$$\left(\frac{\Delta T}{\Delta t}\right)_d(\lambda,\phi,t) = \frac{\Delta T}{\Delta t} - \left(\frac{\Delta T}{\Delta t}\right)_h - \left(\frac{\Delta T}{\Delta t}\right)_v \quad (4)$$

with $(\frac{\Delta T}{\Delta t})_d$ representing the temperature change rate due to the diabatic process and $\frac{\Delta T}{\Delta t}$ the daily mean temperature tendency. Some caution is required for interpreting such temperature change rates when the diabatic process is determined as a residual term (Sousa et al., 2018; Wright and Fueglistaler, 2013). Sub-grid turbulent mixing, analysis increments and other numeric errors may contribute to affect the residual term. For more details see Sousa et al., 2018. The data used to compute the advection and temperature change rates (Eqs. (2)–(4)) were ERA-Interim reanalysis fields at 1000 hPa at 6-hourly output frequency.

3. Results

3.1. Observed and expected mortality

Fig. 1 shows the geographical localization of the Metropolitan Region of Rio de Janeiro (MRRJ) within Rio de Janeiro State and Brazil. According to the 2010 population census performed by the Brazilian Institute of Geography and Statistics, in Portuguese – "Instituto Brasileiro de Geografia e Estatística (IBGE)", around 16 million individuals were living in Rio de Janeiro State, with 74% of this population (nearly 11 million people) concentrated within the MRRJ. These numbers define MRRJ as one of the most densely populated urban areas in South America, and the second most populated metropolitan region in Brazil, after the metropolitan region of São Paulo.

The evolution of the mortality record for the MRRJ during 2000–2015 (Fig. 2), considering all deaths for all age groups and both genders, shows a seasonal cycle with high levels during the winter (June to August), in accordance with previous studies (Carmona et al., 2016; Falagas et al., 2009). However, high mortality peaks are noticed for several years during the summer (December to February) and are likely to be associated with extremely hot events. The 2010 summer was characterized by several of these excessive mortality peaks (Fig. 3). By far, the most remarkable peak in this 16-year record was recorded during the period from 7 to 9 February. On February 9, a total of 414 deaths were recorded, representing an excess of 151 cases when compared to the expected daily average values of 263 deaths for the MRRJ. This period coincided with a sequence of days when the daily Tmax values exceeded the 90th Tmax percentile values. In fact, the 90th percentile value was exceeded in all days of the week 2–9 February, defining an 8-days long HW event (Fig. 3). During February 8, the preceding day of the highest mortality rate, the maximum temperature reached 39 °C in the Galeão meteorological station. Such one-day lag time response between the observed peak temperature and expressive increase in mortality has been interpreted as the time needed for some diseases and pre-existing illnesses to aggravate and cause human deaths (Son et al., 2016). Therefore, to accommodate this temporal lag, we have evaluated the mortality data considering a slightly longer window (2–11 February) than the one used to classify the

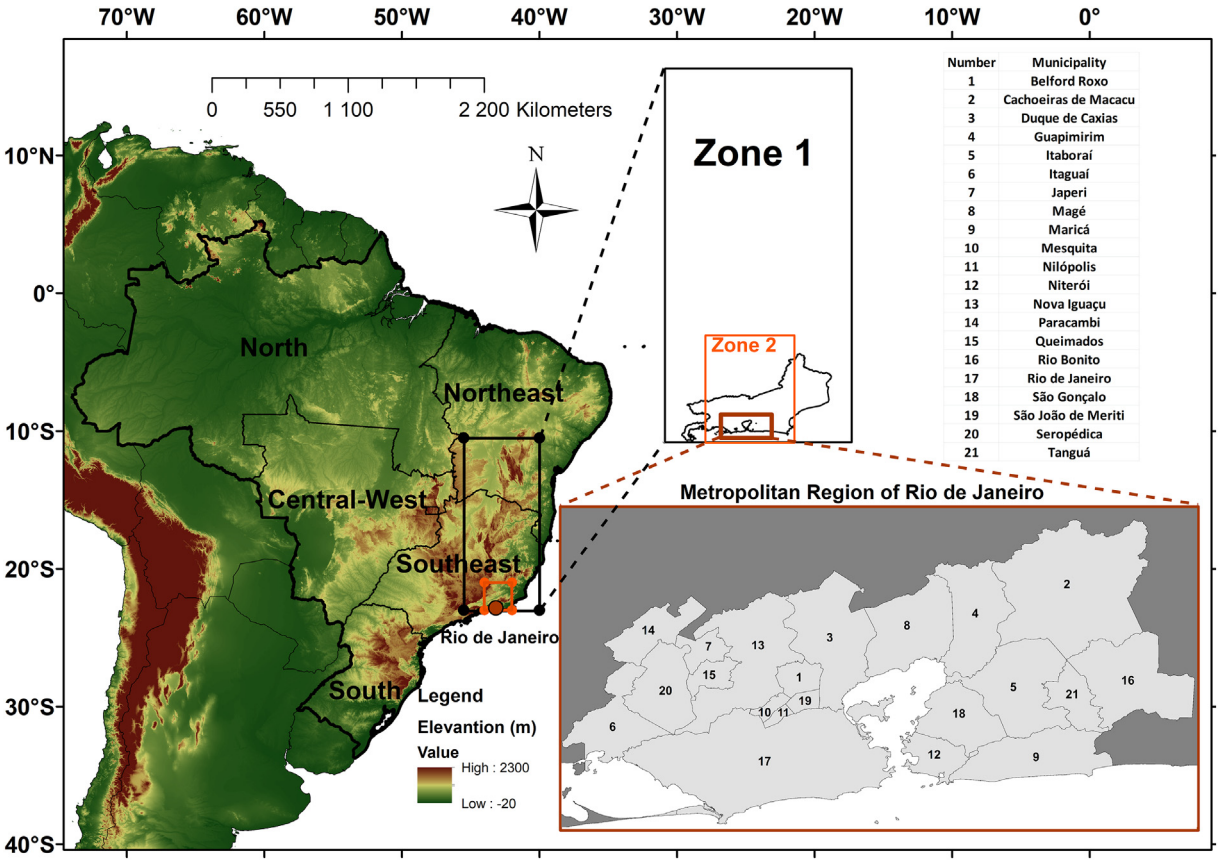

Fig. 1. Map of South America highlighting the Brazil border (bold black line), the five main Brazilian geographical regions (black thin lines: North, Northeast, Central-West, Southeast and South), the state of Rio de Janeiro (brown dot) and two distinct zones (zone 1/black rectangle: 10°–23° S, 40°–45° W; zone 2/orange rectangle: 21°–23° S, 42°–44° W), which are zoomed on the right inset. Representation of Rio de Janeiro state within the zone 1 and 2 and of metropolitan region of Rio de Janeiro with its several municipalities identified by numbers and corresponding names within the top right table.

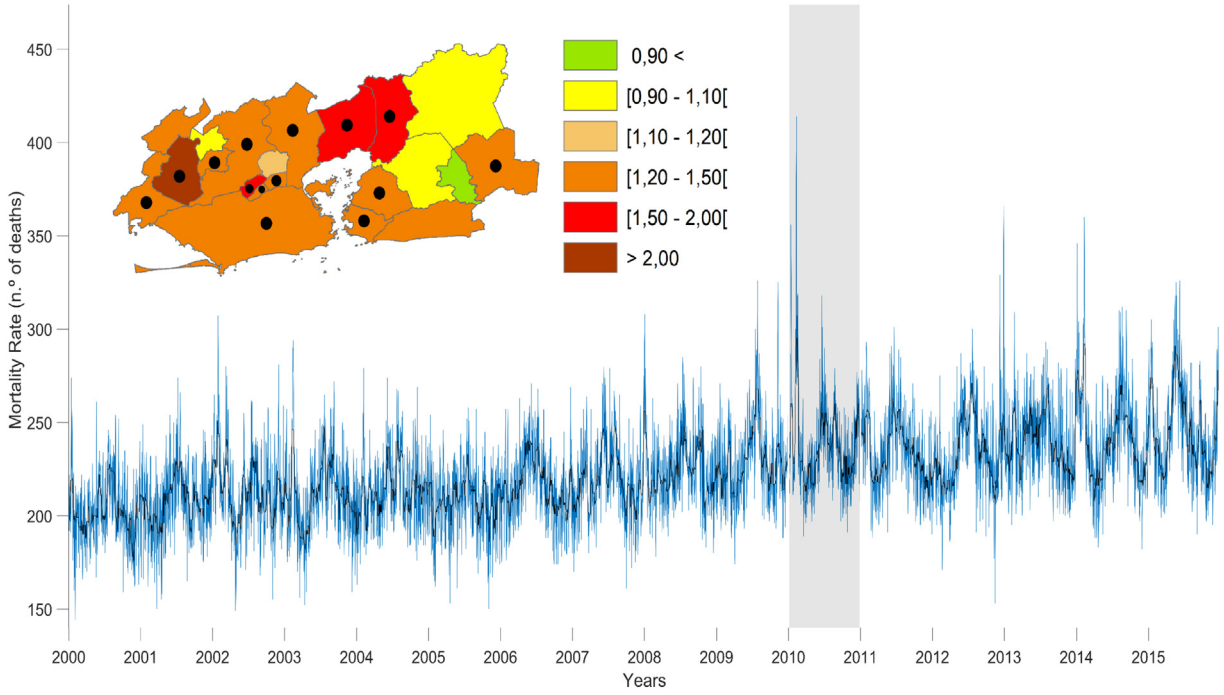

Fig. 2. Mortality Rate time series for the Metropolitan Region of Rio de Janeiro during the period 2000–2015, for total population (blue line) and its 15-day window moving average (black line). The vertical grey bar highlights the 2010 year. The top-left figure represents the values of O/E ratio during the heat wave period and for the several MRRJ municipalities identified on Fig. 1. Black dotes identify districts with statistical significant O/E ratio values at a significance level of 10%.

meteorological HW (2–9 February). Concerning the Tmin, during the HW period the values were about 23 °C–24 °C, i.e. temperatures that fall very close to the 90th percentile, but do not exceed it (Fig. 3). Nevertheless, these high values were capable, in conjunction with the extreme Tmax values, to induce considerable heat stress in human body's inhibiting a normal night-time cooling relief period.

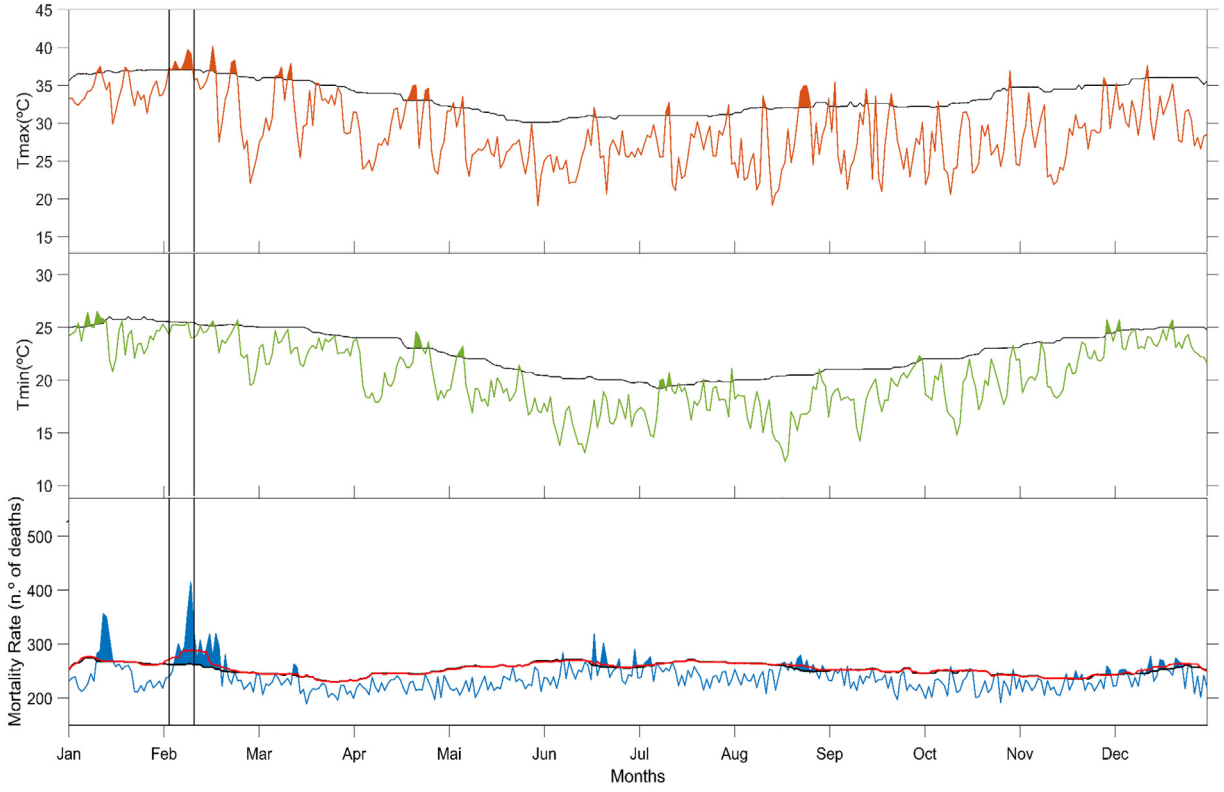

Fig. 3. Daily Tmax, Tmin and Mortality Rate values for the year of 2010 (top, middle and bottom panels respectively). The black line represents the respective climatological (1961–2014 for Tmax and Tmin; 2000–2015 for Mortality) calendar day 90th percentile calculated on a 15-day window (centered on the day in question). For Mortality panel, the black line represents the climatological calendar day 90th percentile computed excluding the year of 2010 while the red line represents the same 90th percentile computed using all the analysis period, and so, including the year of 2010.

Table 1
Observed (O) and expected (E) deaths for the period 2–11 February 2010. Estimates of excess deaths (O-E) and O/E ratio are also shown. Expected mortality computed using the 2000–2015 period. All results are split by gender and agree group. *p* refers to the significance level.

	Observed deaths (O)		Expected deaths (E)		Excess of deaths (O-E)		O/E		*p*-Value	
Women	1624		1130		494		1,44		<0,001	
Men	1382		1139		243		1,21		<0,001	
Total	3006		2269		737		1,32		<0,001	
Age groups	W	M	W	M	W	M	W	M	W	M
0–14	40	45	38	51	2	-6	1.05	0.88	0,800	0,400
15–29	17	30	19	28	-2	2	0.89	1.07	0,600	0,700
30–59	269	342	240	330	29	12	1.12	1.04	0,100	0,500
≥60	1298	965	833	729	465	239	1.56	1.32	<0,001	<0,001

During the 10-day period spanning from 2 to 11 February, a total of 3006 deaths were recorded in the MRRJ, which represented an excess of approximately 737 deaths and an O/E ratio of 1.32 (Table 1). The ratio O/E was larger than unit and statistically significant at 1% level, indicating more deaths than expected. It was higher for female (1.44) than for male (1.21). Regarding age groups, the elderly (60 years old or older) were the ones presenting the highest mortality (2263 deaths), which represented 75% of all deaths recorded during the HW period. The O/E ratio was also more pronounced for elderly women (1.56) than for elderly man (1.32), evidencing an asymmetrical gender risk in accordance to previous analysis (Nogueira and Paixão, 2008; Yu et al., 2010). A similar situation was observed for the 30–59 and 0–14 age groups. For both Male and Female groups, the O/E ratio was only statistically significant at 1% level regarding the elderly population group. Analyzing Fig. 2 and the O/E ratio values for total population disaggregated for the several MRRJ municipalities, we observed that only one district recorded an O/E ratio lower than 0.90 (Tanguá). From the total 21 MRRJ municipalities, 14 presented statistically significant positive ratios. The highest ones were recorded for Seropédia (>2.0) followed by Mesquita, Magé and Guapimirim which recorded values between 1,5 and 2. The reason for the record of high mortality risk values in these particular districts is probably related to a high number of elderly people with low social-economic conditions living within them. Other external factors as the access of quality public health services can be also a plausible explanation.

3.2. Atmospheric synoptic characterization

This section aims to define the large-scale and regional atmospheric mechanisms contributing to the HW development. This characterization was performed through the analysis of anomaly composite fields of several meteorological variables, with anomalies computed with respect to the 1979–2014 period. The robustness of these anomaly composites was evaluated using a two-tailed *t*-test to access the statistical significance at the 1% level of the difference between the 2–9 February 2010 composite field and the long term summer (DJF) climatology. An important consideration to be made concerns the fact that during the period 1979–2014 temperature trends were recorded. The temporal analysis of this HW episode covers the year of 2010 which is a time period that corresponds to a final segment of the 1979–2014 period. Consequently, statistical significant anomalies are more likely to be found. In order to minimize this effect in our results, we increased the rigor of the statistical test using a significance level of 1%. Alternative approaches to deal with temperature trends when defining extreme events include considering time-varying thresholds as in Coelho et al. (2008) and computing anomalies using moving climatologies as in Coelho and Goddard (2009).

3.2.1. Large-scale anomalies

Fig. 4 illustrates the upper troposphere (250 hPa) 2010 HW fingerprint through the geopotential height (H250, contours) and meridional wind component (V250, shaded) anomalies for the period 2–9 February 2010. The anomaly field for both atmospheric variables highlights a statistically significant wave train pattern, which spans from the central/east south Pacific Ocean to South America, suffering a northward deflection east of the Andes mountain range. This stationary wave pattern is characterized by a sequence of alternating positive/negative anomalous meridional wind centers, associated with the establishment of several near concentric anomalous geopotential height centers. The initial signs of development of such wave pattern were identified during the first days of 2010 (not shown). Afterwards and during January, it maintained its developing status presenting its most matured stage later during the HW event. As a consequence of this upper atmospheric level wave flow, a quasi-stationary anticyclonic system was observed over

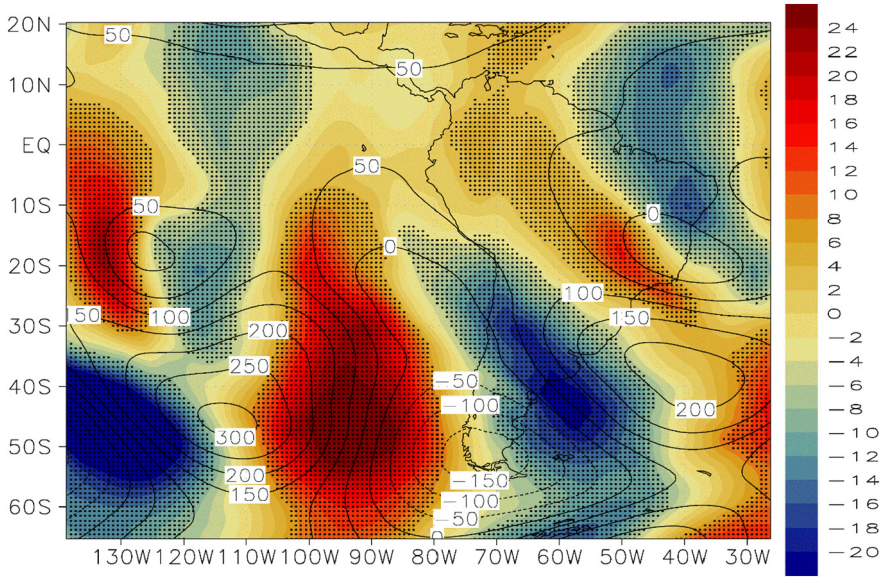

Fig. 4. Averaged 250 hPa v-wind (shaded, ms^{-1}) and 250 hPa Geopotential height anomaly fields (contours, gpm) for the period 2–9 February 2010. Black dotes denote statistically significant (at the 1% level) grid-points of the 250 hPa v-wind anomaly field regarding summer (DJF) climatology, through a two tailed *t*-test.

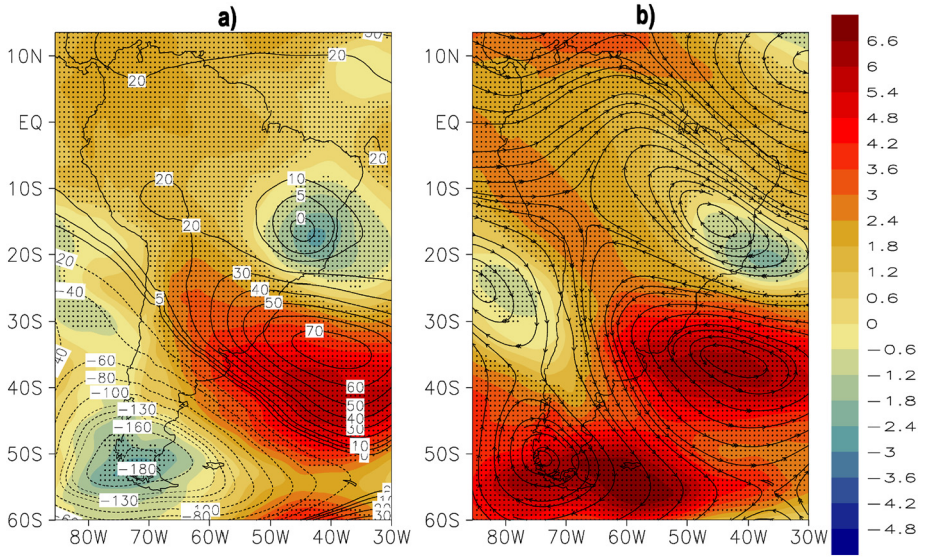

Fig. 5. Averaged 500 hPa temperature (shaded, °C) and 500 hPa Geopotential height anomaly fields (contours, gpm) for the period 2–9 February 2010 (a). Averaged 250 hPa temperature (shaded, °C) and streamlines for the period 2–9 February 2010 (b). Black dots denote all grid-points of both 500 hPa and 250 hPa temperature anomaly field that are statistically significant at the 1% level regarding summer (DJF) climatology, through a two-tailed *t*-test.

the South Atlantic Ocean and near the Brazilian coast, where a large-scale positive H250 anomaly center was located. This anomalous atmospheric circulation with a quasi-barotropic structure influenced the meteorological anomalies observed at the surface during the HW period.

The geopotential height anomaly at 500 hPa (H500) shown in Fig. 5a, highlights an intense and well-marked concentric anomaly that is relatively coincident with the previously noticed positive geopotential height anomaly at the 250 hPa level (H250). Maximum anomalies of 70 gpm were recorded over the South Atlantic Ocean, southeast of the Brazilian coastline, evidencing the quasi-barotropic nature of this structure. Both H500 and H250 anomalies apparently resulted from a large-scale teleconnection between the South Pacific and South Atlantic Oceans and have already been identified in previous studies dealing with climatic extremes in southeastern Brazil (Coelho et al., 2016; Liebmann et al., 2004). Positive 500 hPa temperature anomalies (T500) were also widespread but slightly offset to the southwest of the H500 positive anomaly. This is a typical signature of a large-scale permanent anticyclonic circulation, a situation previously associated with SEB HW events (Geirinhas et al., 2017). To the north of Rio de Janeiro, an almost circular core structure characterized by much reduced positive H500 anomalies (compared to the surrounding values) was observed and accompanied by negative T500 anomaly values.

Analyzing the temperature field, as well as the streamlines, for the 250 hPa level and for the same region (Fig. 5b), it was possible to verify a very similar scenario. Thus, a negative T250 anomaly core was identified, embedded on a pronounced cyclonic circulation pattern, which is a typical scenario associated with the establishment of an upper tropospheric cyclonic vortex. The north-south positioning over the eastern side of South America of both cyclonic and anticyclonic anomalies promoted a meridional separation of the westerly zonal flow. Such bifurcation occurred over the northwest South America (10–15°S), over the region where the Bolivian High system is usually located during summer (Fig. 5b) (Lenters and Cook, 1997). As a consequence, the zonal tropical jet stream suffered a considerable weakening (Archer and

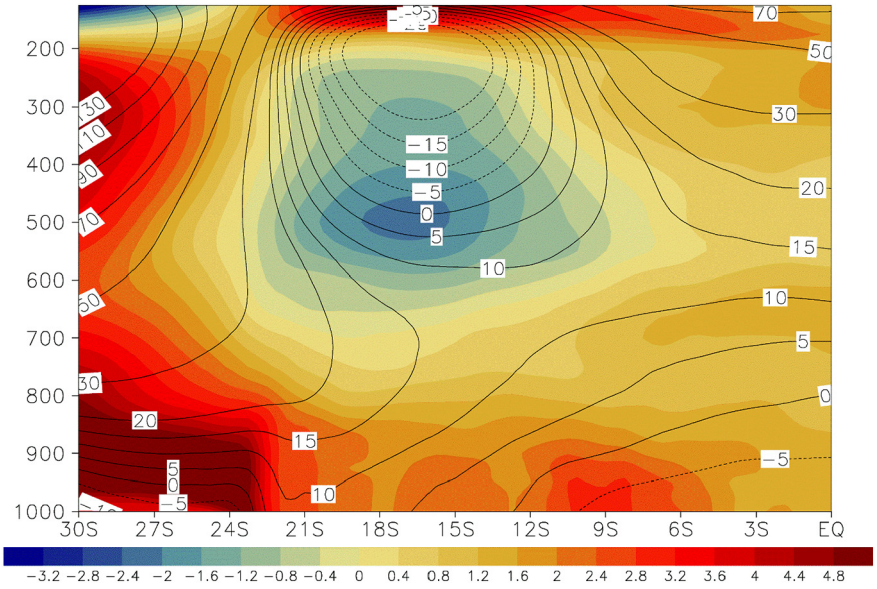

Fig. 6. North – South Vertical Section at 45°W Longitude. Anomaly field for the period 2–9 February 2010 of Temperature (shaded, °C) and of Geopotential height (contour, gpm).

Caldeira, 2008). To better understand this phenomenon, we have analyzed a North-South vertical section of the temperature and geopotential height anomaly at 45°W longitude during the HW period (Fig. 6). This figure shows the signature of this cold upper-level tropospheric vortex throughout the establishment, between 24°S and 9°S, of negative anomalies of both temperature and geopotential height for most the upper levels of the troposphere (200–600 hPa). Temperatures near the surface were unaffected by the presence of the vortex and were instead affected by the anticyclonic conditions noticed over southern regions.

3.2.2. Regional surface anomaly fields

The anomalous surface wind pattern observed over SEB (Fig. 7) is coherent with the presence of a quasi-stationary anticyclonic circulation. Near 20°S and between 55°W and 65°W, there is an intense anomalous southward flow strengthening the so-called South American Low-Level Jet (SALLJ), and consequently increasing the moisture transport from the Amazon basin to southern Brazil (Marengo et al., 2004; Nogués-Paegle and Mo, 1997). Overall, the anomaly field of near-surface wind reveals an advection of air masses towards southeastern and southern Brazil coastal areas. These regions, together with the upper Paraná basin, were characterized by the highest positive Tmax anomalies of around 5–6 °C (Fig. 7a). The anticyclonic circulation also promoted the development of clear sky conditions with positive SRad anomalies (Fig. 7b) and, consequently, both negative RHsfc (Fig. 7c) and Prec (Fig. 7d) anomalies over most SEB. However, a comparison of Tmax and SRad spatial patterns indicates that the SRad and diabatic heating mechanisms are not sufficient to explain the location of the highest Tmax anomalies over the coastal areas and the upper Paraná basin (Fig. 7a). On the contrary, negative (positive) SRad (RHsfc) anomalies were observed within 30–35°S and 55–65°W, a situation already identified in HW studies for SEB (Geirinhas et al., 2017).

This enhanced positive RadS anomaly together with exceptionally dry conditions contributed to the identified statistically significant negative SoilW anomalies over SEB, particularly in the meridionally (S-N) oriented band, extending from Rio de Janeiro northwards into

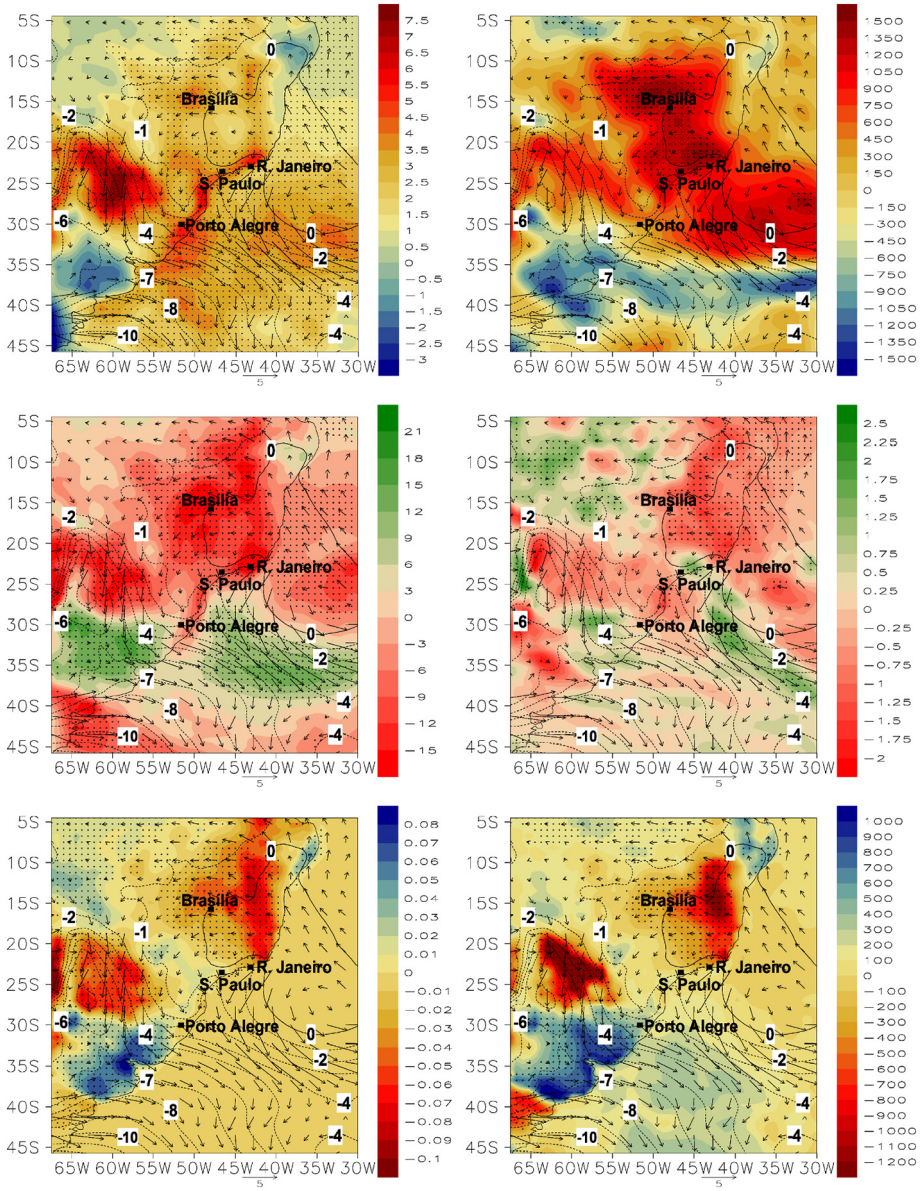

Fig. 7. Averaged anomaly fields for the period 2–9 February 2010 of SLP (contour, hPa), wind 10 m height (vectors, ms^{-1}) and of (a) Tmax (shaded, °C), (b) RadS (shaded, $W\,m^{-2}$), (c) HRsup (shaded, %), (d) Prec (shaded, mm), (e) SoilW (shaded, m^3_{H2O}/m^3_{soil}), (f) SH (shaded, $W\,m^{-2}$). Black dotes denote all grid-points of the meteorological anomaly field represented in shaded that are statistically significant at the 1% level regarding summer (DJF) climatology, through a two-tailed *t*-test.

continental regions (Fig. 7e). This SEB sub-region also presented significant positive SH anomalies (Fig. 7f), a situation expected considering the land-atmosphere energy fluxes that occur when such extreme SRad and SoilW conditions are observed (Fischer et al., 2007; Miralles et al., 2014). Due to the presence of a northerly surface flow near Rio de Janeiro (Fig. 7a), dry and warm air coming from this meridional band region northward Rio de Janeiro was steadily advected towards MRRJ during the 2010 HW period.

Pronounced dry soil conditions such as the ones observed during the HW are usually a result of an extended period of severe Prec and RHsfc deficits, accompanied by strong radiative anomalies due to clear sky conditions (Ferranti and Viterbo, 2006; Fischer et al., 2007). To evaluate the validity of such hypothesis, Fig. 8 shows the evolution of both these variables, for several sub-sample periods within January and February, using the mean interquartile range boxes, using data for the 1979–2014 period. The darkest (lighter) grey boxes correspond to average values throughout the zone 1 (2) previously defined in Fig. 1. Zone 1 corresponds to the large meridional oriented region within SEB (Fig. 1), where positive SoilW and SH anomalies were pronounced and from where the air was transported towards the MRRJ during the HW period (Fig. 1). Zone 2 encompasses the MRRJ and its surroundings (Fig. 1). The observed values during 2010 are also shown in Fig. 8 with corresponding black and grey circles. Tmax values during 2010 were exceptionally high during the period from January 1 to February 16 for both zones (Fig. 8a). In zone 1, Tmax and SRad maximum values were reached before the 2010 HW event, between January 26 and February 1, while in zone 2 the peak values were recorded during the HW period. SRad values during 2010 were also continuously recorded above the median for both zones and close to record values in zone 2 (Fig. 8b). On the other hand, the evolution of SoilW values during the 2010 show a well-marked negative trend for both areas throughout January and February (Fig. 8c), with minimum record values observed in zone 1 during the HW, while the lowest values in zone 2 were recorded just after the HW period, i.e., during February 10–16. The evolution of SH shows very similar patterns for both sectors as the one verified for SoilW. Strong land-atmosphere positive energy fluxes were permanent from January 1 until the end of HW period, especially in zone 1 and during the HW preceding days, a scenario that contributed to the re-amplification of surface temperature anomalies.

3.2.3. Physical air heating mechanisms

Tmax and SRad anomaly fields do not entirely match (Fig. 7), indicating that diabatic heating processes were not the only mechanism contributing to the abnormal high Tmax values recorded during the HW period. Several physical processes, such as diabatic heating and horizontal/vertical advection mechanisms, are compatible with atmospheric anticyclonic circulation patterns (see Eqs. (2)–(4)). In this section, we envisage determining which of these mechanisms played the primary role for the observed heat stress during the HW event.

Fig. 9 shows the temporal evolution of the contribution of each of these physical mechanisms to the 1000 hPa temperature (T1000) anomaly in MRRJ during the period from January 27 to February 19, encompassing a pre and a post HW period. Overall this time window was characterized by positive (above average) T1000 anomalies which reached their highest values for several consecutive days during the HW period (Fig. 9). During the period encompassing pre and post HW conditions, the daily evolution of the horizontal advection contribution term (Fig. 9 bottom panel, blue curves) was generally negative (as well as the cumulative contribution). The daily diabatic contribution (Fig. 9 bottom panel, red curves) term showed three distinct periods of abnormal positive values, where diurnal diabatic heating was considerably higher than the radiative cooling during night time. The HW period was one of these three periods, however, the most pronounced one was observed after February 15. In general, the daily vertical advection

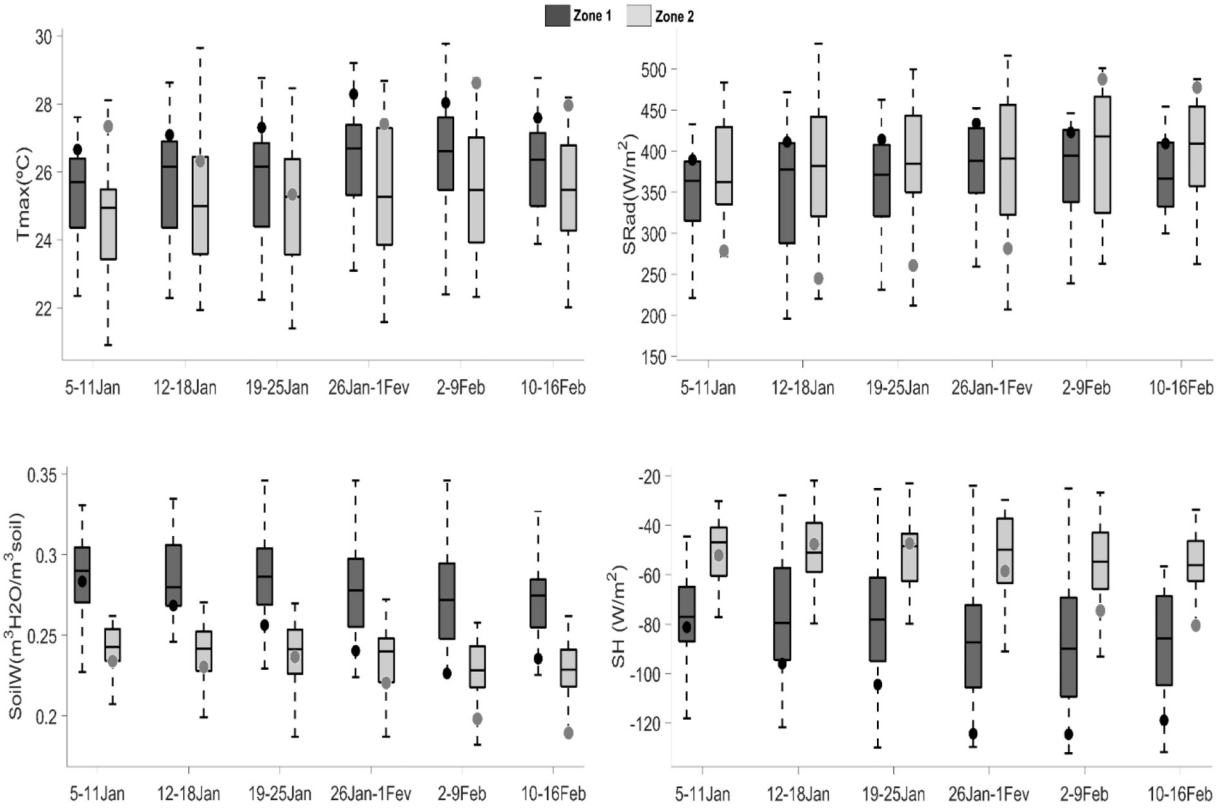

Fig. 8. Boxplots (1979–2014 base period) for weekly periods within January and February and for the HW period (2–9 February) of (a) Tmax (°C), (b) RadS ($W\,m^{-2}$), (c) SoilW ($m^3_{H2O}.m^{-3}_{soil}$) and SH ($W\,m^{-2}$). Boxes correspond to the interquartile range and whiskers correspond to the extreme values for the entire base period. The black (grey) boxes represent averaged values over the zone 1 (zone 2), which are geographically identified in Fig. 1. The circles represent the corresponding averaged weekly values observed for the year of 2010.

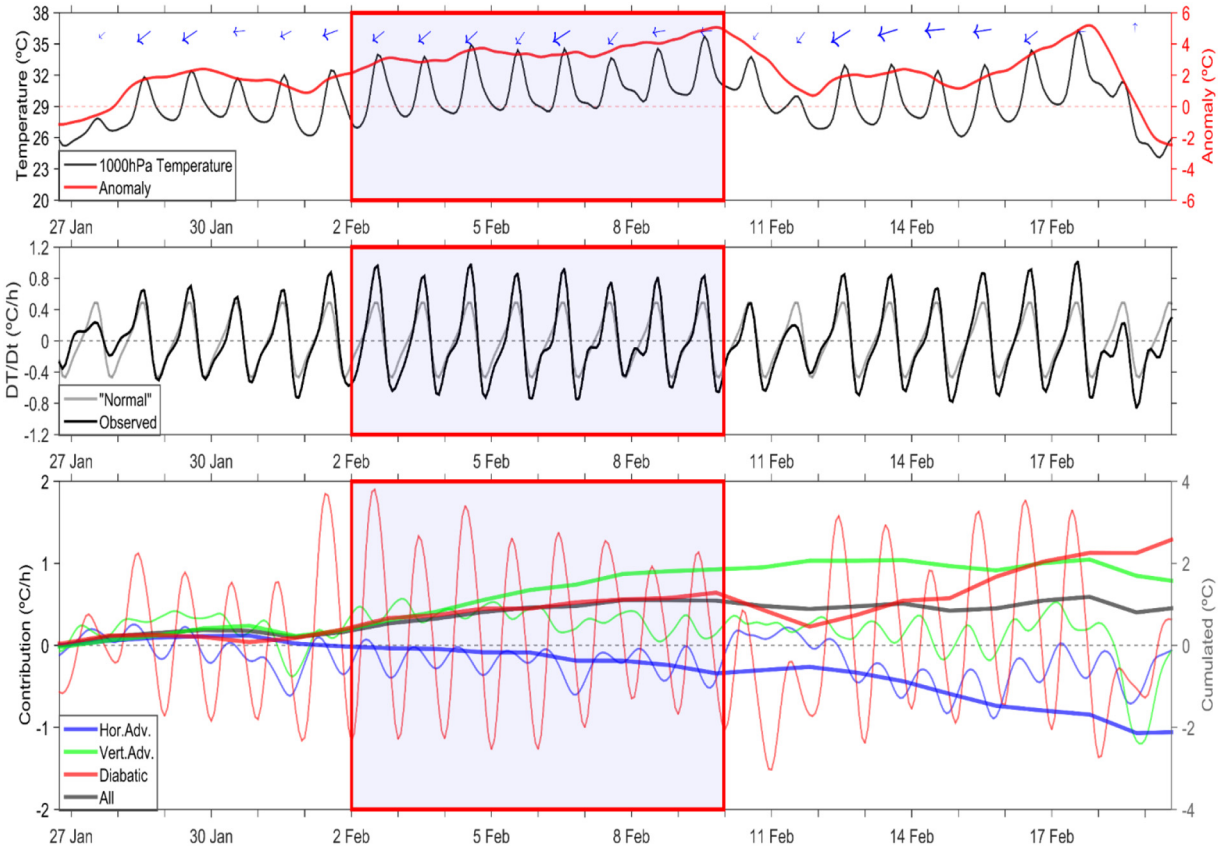

Fig. 9. Temporal evolution throughout January 27 and February 19 of 2010 of several meteorological and physical parameters for the MRRJ. The red boxes delimit the heat wave period under analysis. Top panel: evolution of wind pattern (blue arrows), observed 1000 hPa Temperature (black curve) and the associated anomaly (red curve) with respect to the corresponding calendar day climatology (1979–2014); Middle panel – Evolution of the expected (1979–2014) 1000 hPa temperature variation rate (grey curve) and the observed values during 2010 (black curve); Lower panel – evolution of the contribution of the horizontal advection (blue lines), vertical advection (green lines) and diabatic (red lines) terms and of their combined contribution (black line) for the observed 1000 hPa temperatures anomalies. Each ticker line represents the respective cumulated contribution term.

contribution term presented positive values (Fig. 9 bottom panel, green curves), in particular during the HW episode. A marked increase in the cumulative curve during this period (above the two other contribution terms) indicates that, despite the critical role played by diabatic heating, the primary physical mechanism responsible for the abnormally high temperatures that occurred during the 2010 HW event was the adiabatic heating via vertical advection (enhanced subsidence). Pronounced positive values of vertical advection contribution term during the HW also match the period where the northerly wind component over the MRRJ was more pronounced. Fig. 10 represents (black crosses) the regions where the vertical advection contribution term was predominant for T1000 anomalies. Similarly to MRRJ, the positive surface temperature anomalies recorded during the HW period in the south and southeast Brazilian coastal regions were mainly a product of enhanced subsidence processes. Analyzing the topography (Fig. 10), it is possible to note that these coastal areas are surrounded by mountain regions upstream of the observed flow. The surface wind anomaly pattern indicates a strong advection of dry and relatively warm air from interior high regions towards coastal areas including MRRJ (Figs. 7 and 10). These katabatic winds (at the synoptic scale) promoted by the anticyclonic circulation resulted in abrupt air compression and consequently in the adiabatic heating mechanism, explaining the regional coastal strip of striking temperature anomalies.

4. Discussion and conclusions

This study characterized in detail the atmospheric circulation and physical mechanisms contributing to the development of a prolonged period with excess heat in the MRRJ, which ultimately led to the highest mortality rate recorded in a recent 16-year period (2000–2015). Recent studies have shown that mortality rates tend to increase considerably when expressively above normal Tmax values are observed for consecutive days and aggravated by concurrent high Tmin temperature values, inhibiting a normal night-time cooling relief period (Anderson and Bell, 2009; Gasparrini and Armstrong, 2012). Exploring the HW effects on mortality values and considering gender and age groups, a higher risk was identified for women compared to men particularly for the elderly. A remarkable total number of 737 deaths were potentially related to excess heat conditions. All these results corroborate previous studies developed for other extremely hot events in Central and South Europe during 2003 and 2006 (Trigo et al., 2005; Filleul et al., 2006; Vandentorren et al., 2006; Robine et al., 2008; Trigo et al., 2009). Other unaccounted social-economic factors such as population awareness for health impacts induced by extreme heat conditions, access to health care, nutrition and housing thermal comfort, are also relevant for determining and interpreting mortality risk. Thus, for a more in-depth mortality analysis, a careful social-economic population characterization, and a more detailed analysis focusing on the main heat-related diseases (respiratory, cardiovascular illnesses) should be carried out to support public health authorities implementing effective and adequate preventive measures.

Concerning the large-scale atmospheric circulation scenario associated to the development of this HW event, a quasi-stationary Rossby wave train, embedded in the westerly flow, was formed and matured during January 2010, persisting until the HW period (2–9 February 2010). Previous studies have shown that when such u-shaped wave-

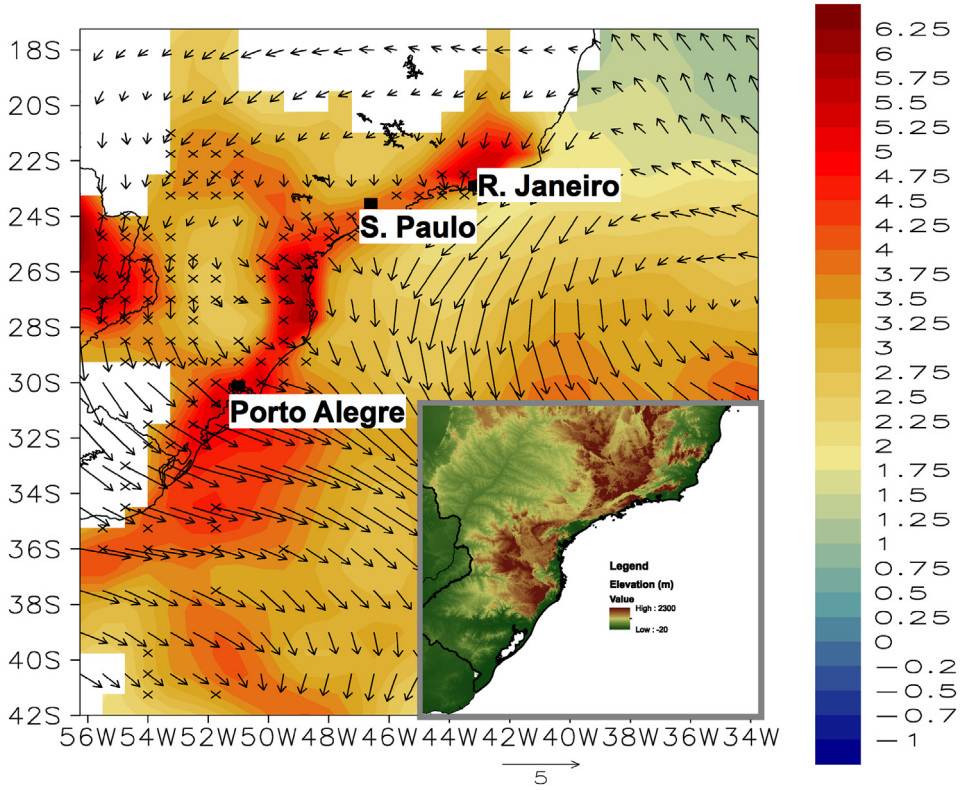

Fig. 10. Averaged anomaly field of Tmax (shaded, °C) and of wind 10 m height (black arrows, ms^{-1}) regarding the 2–9 February 2010 period. Regions where the surface temperature anomaly was mainly result of the vertical advection mechanisms are represented by black crosses. The Tmax anomaly values that are not statistically significant at the 1% level are not colored. On the right bottom corner, a small inset panel represents the same Brazilian land section, depicting the respective spatial distribution of elevation values (m).

like pattern is established, persistent atmospheric anticyclonic conditions tend to develop over the South Atlantic Ocean, fostering pronounced hot and dry periods over the SEB region (Cerne and Vera, 2011; Coelho et al., 2016; Liebmann et al., 2004). This wave train is a signature of a teleconnection pattern between the Southeast Pacific Ocean, South America and the South Atlantic Ocean, the so-called Pacific – South America Modes (Renwick and Revell, 1999; Mo and Paegle, 2001; Irving and Simmonds, 2016). These modes are excited over central/east south Pacific Ocean in association with anomalous SST and can be directly related to El-Niño-Southern Oscillation (ENSO) episodes, more specifically those whose SST anomalies are confined to the central Pacific Ocean (Coelho et al., 2016). In fact, during the 2009–2010 temperature record-breaking in the MRRJ anomalously warm SST's were observed over a confined central Pacific area (Kim et al., 2011), a scenario that has been more frequent in recent decades and classified as warm pool El Niño events (Kug et al., 2009). Thus, the quasi-stationary mid-atmospheric anticyclonic anomaly over the South Atlantic during the HW period may be attributed to a large extent to the remote forcing of an anomalous SST pattern over the central Pacific Ocean. Northward of Rio de Janeiro, a cold core vortex in the upper tropospheric, with a vertical extend down to 500 hPa, was present during the HW period. This type of upper-level atmospheric structure can be found more frequently between 25 and 45°W and 10–25°S during the austral summer, with January being the month of maximum peak activity (Kousky and Alonso Gan, 1981). Although not shown here, we observed that the vortex developed over the northeast coast of Brazil during the first days of January 2010 as a consequence of an anticyclonic anomaly located just south of the Brazilian coast. The release of large amounts of latent heat by the SACZ intensifies the anticyclonic center in altitude promoting the development of a cyclonic structure in an attempt to preserve the absolute vorticity. Due to a lack of dissipative mechanisms, this closed cyclonic structures can last for weeks (Kousky and Alonso Gan, 1981). At the lower tropospheric levels, the central region of these vortices is often characterized by air subsidence and clear sky conditions (Frank, 1970). This central vortex region located northward of Rio de Janeiro matched well with the area characterized by maximum values of shortwave radiation incidence during the HW event, and where the driest soil conditions were verified.

We also show the relevance of soil-atmosphere feedback mechanisms in the development of the HW. For the period spanning from January 2010 to the HW occurrence, large values of shortwave radiation incidence at surface were observed over the SEB and some central and northeastern Brazil areas. Climatologically, the SEB region experiences the highest precipitation rates during the austral summer in association with the occurrence of the South Atlantic Convergence Zone (SACZ) events, which are characterized by a well-defined enhanced cloud cover band (northwest-southeast oriented) fed by moisture advected from the Amazon region by the SALLJ (Herdies et al., 2002). Wet SACZ events over SEB depend on the interaction between extra-tropical frontal systems and the tropical convection over this region. Therefore, a southward deviation of cyclonic tracks is directly related to reduced precipitation over SEB. The observed persistent mid-level anticyclonic circulation offsets the SACZ influence over SEB, while the SALLJ was intensified further south. Consequently, a more southward moisture transport from the Amazon basin was imposed towards the region of La Plata Basin (Berbery and Barros, 2002; Liebmann et al., 2004).

On the other hand, persistent shortwave radiation anomalies over SEB and central Brazil during January 2010 contributed to accelerating soil drying through great evaporation rates, resulting in a positive feedback mechanism that promoted the amplification of the hot and dry surface conditions, especially to the north of the MRRJ. A similar mechanism was identified and well documented during the 2003 European mega HW, where extreme surface temperatures were manifested due

to land-atmosphere positive feedbacks that affected the extent of the geopotential height anomaly (Fischer et al., 2007).

On a final and regional stage, pronounced elevation differences between the interior and coastal areas resulted in katabatic winds. Thus, downstream, from the MRRJ to Porto Alegre, strong adiabatic heating of the already warm air mass previously formed upstream by diabatic processes and land-atmosphere feedbacks during January, occurred at lower elevations. The positive adiabatic contribution to surface heating throughout this narrow coastal region overwhelmed the net diabatic heating and the horizontal cooling advection associated to usual coastal sea breezes.

Summing up, this severe HW event in the MRRJ was driven by atmospheric processes at different time and spatial scales. Several abnormal atmospheric/land conditions were identified during the preceding weeks. The identification of Pacific abnormal SST's during a warm-pool El Niño event, capable of generating a similar Rossby Wave train, should be diagnosed as a signal for the development of potential relatively hot and dry conditions in the MRRJ, particularly after a drier than normal spring. The detailed characterization presented for this severe heat event should be taken into account when looking into medium range meteorological forecasts (up to 10–15 days) for the MRRJ. To our best knowledge, works of this kind were already develop for other global regions, however, for Rio de Janeiro and for this specific region of SEB this is a pioneer analysis. Thus, equivalent detailed atmospheric analyses for other Brazilian areas should be carried, especially for northern sectors, where pronounced increasing temperature trends are expected according to recent robust climate change scenarios (IPCC, 2014), and where the Brazilian population group with the lowest wealth per capita and education levels currently live (Costa et al., 2015). It is also expected that population size, mainly elderly people living in large urban centers, is likely to increase in future. The elderly population in 2000 in the MRRJ was 11,7% of the total population. In 2010 this number increased to 15,8% and is expected to continue increasing (IBGE, 2010). This study is particularly relevant for authorities to minimize the future human impacts of climate change allowing society to adapt to a range of different climate change scenarios, with the most likely ones (RCP4.5 till RCP 8.5) being characterized by more frequent extreme heat stress conditions.

Acknowledgments

JG was supported by The Navigator Company project. RL was supported by Serrapilheira Institute (grant number Serra-1708-15159). CASC was supported by CNPq, process 304586/2016-1. We also acknowledge the support provided by FAPERJ, respectively, by the Visiting program funded (E-26/200.636/2016) and the Thematic program (E-26/210.904/2016), FAPESP-FCT project BrFLAS (1389/2014, 2015/01389-4), and FAPESP CLIMAX project (2015/50687-8).

References

Anderson, B.G., Bell, M.L., 2009. Weather-related mortality: how heat, cold, and heat waves affect mortality in the United States. Epidemiology 20, 205–213. https://doi.org/10.1097/EDE.0b013e318190ee08.

Archer, C.L., Caldeira, K., 2008. Historical trends in the jet streams. Geophys. Res. Lett. 35, L08803. https://doi.org/10.1029/2008GL033614.

Åström, D., Bertil, F., Joacim, R., 2011. Heat wave impact on morbidity and mortality in the elderly population: a review of recent studies. Maturitas 69, 99–105. https://doi.org/10.1016/j.maturitas.2011.03.008.

Barnett, A.G., 2007. Temperature and cardiovascular deaths in the US elderly: changes over time. Epidemiology 18, 369–372. https://doi.org/10.1097/01.ede.0000257515.34445.a0.

Barriopedro, D., Fischer, E.M., Luterbacher, J., Trigo, R.M., García-Herrera, R., 2011. The hot summer of 2010: redrawing the temperature record map of Europe. Science 332 (80), 220–224. https://doi.org/10.1126/science.1201224.

Bastos, A., Gouveia, C.M., Trigo, R.M., Running, S.W., 2014. Analysing the spatio-temporal impacts of the 2003 and 2010 extreme heatwaves on plant productivity in Europe. Biogeosciences 11, 3421–3435. https://doi.org/10.5194/bg-11-3421-2014.

Basu, R., Samet, J.M., 2002. Relation between elevated ambient temperature and mortality: a review of the epidemiologic evidence. Epidemiol. Rev. 24, 190–202. https://doi.org/10.1093/epirev/mxf007.

Bell, M.L., O'Neill, M.S., Ranjit, N., Borja-Aburto, V.H., Cifuentes, L.A., Gouveia, N.C., 2008. Vulnerability to heat-related mortality in Latin America: a case-crossover study in São Paulo, Brazil, Santiago, Chile and Mexico City, Mexico. Int. J. Epidemiol. 37, 796–804. https://doi.org/10.1093/ije/dyn094.

Berbery, E.H., Barros, V.R., 2002. The hydrologic cycle of the La Plata Basin in South America. J. Hydrometeorol. 3, 630–645. https://doi.org/10.1175/1525-7541(2002)003<0630:THCOTL>2.0.CO;2.

Bitencourt, D.P., Fuentes, M.V., Maia, P.A., Amorim, F.T., 2016. Frequência, duração, abrangência espacial e intensidade das ondas de calor no Brasil. Rev. Bras. Meteorol. 31, 506–517. https://doi.org/10.1590/0102-778631231420150077.

Braga, A.L.F., Zanobetti, A., Schwartz, J., 2002. The effect of weather on respiratory and cardiovascular deaths in 12 U.S. cities. Environ. Health Perspect. 110, 859–863. https://doi.org/10.1289/ehp.02110859.

Carmona, R., Díaz, J., Mirón, I.J., Ortiz, C., Luna, M.Y., Linares, C., 2016. Mortality attributable to extreme temperatures in Spain: a comparative analysis by city. Environ. Int. 91, 22–28. https://doi.org/10.1016/j.envint.2016.02.018.

Ceccherini, G., Russo, S., Ameztoy, I., Patricia Romero, C., Carmona-Moreno, C., 2016. Magnitude and frequency of heat and cold waves in recent decades: the case of South America. Nat. Hazards Earth Syst. Sci. 16, 821–831. https://doi.org/10.5194/nhess-16-821-2016.

Cerne, S.B., Vera, C.S., 2011. Influence of the intraseasonal variability on heat waves in subtropical South America. Clim. Dyn. 36, 2265–2277. https://doi.org/10.1007/s00382-010-0812-4.

Coelho, C.A.S., Goddard, L., 2009. El Niño-induced tropical droughts in climate change projections. J. Clim. 22, 6456–6476. https://doi.org/10.1175/2009JCLI3185.1.

Coelho, C.A.S., Ferro, C.A.T., Stephenson, D.B., Steinskog, D.J., 2008. Methods for exploring spatial and temporal variability of extreme events in climate data. J. Clim. 11, 2072–2092. https://doi.org/10.1175/2007JCLI1781.1.

Coelho, C.A.S., Cavalcanti, I.A.F., Costa, S.M.S., Freitas, S.R., Ito, E.R., Luz, G., Santos, A.F., Nobre, C.A., Marengo, J.A., Pezza, A.B., 2012. Climate diagnostics of three major drought events in the Amazon and illustrations of their seasonal precipitation predictions. Meteorol. Appl. 19, 237–255. https://doi.org/10.1002/met.1324.

Coelho, C.A.S., de Oliveira, C.P., Ambrizzi, T., Reboita, M.S., Carpenedo, C.B., Campos, J.L.P.S., Tomaziello, A.C.N., Pampuch, L.A., Custódio, M. de S., Dutra, L.M.M., Da Rocha, R.P., Rehbein, A., 2016. The 2014 southeast Brazil austral summer drought: regional scale mechanisms and teleconnections. Clim. Dyn. 46, 3737–3752. https://doi.org/10.1007/s00382-015-2800-1.

Costa, D., Hacon, S., Siqueira, A.S.P., Pinheiro, S.L.L.A., Gonçalves, K.S., Oliveira, A., Cox, P., 2015. Municipal temperature and heatwave predictions as a tool for integrated socio-environmental impact analysis in Brazil. Am. J. Clim. Chang. 04, 385–396. https://doi.org/10.4236/ajcc.2015.44031.

de Barros Soares, D., Lee, H., Loikith, P.C., Barkhordarian, A., Mechoso, C.R., 2017. Can significant trends be detected in surface air temperature and precipitation over South America in recent decades? Int. J. Climatol. https://doi.org/10.1002/joc.4792.

Dee, D.P., Uppala, S.M., Simmons, A.J., Berrisford, P., Poli, P., Kobayashi, S., Andrae, U., Balmaseda, M.A., Balsamo, G., Bauer, P., Bechtold, P., Beljaars, A.C.M., van de Berg, L., Bidlot, J., Bormann, N., Delsol, C., Dragani, R., Fuentes, M., Geer, A.J., Haimberger, L., Healy, S.B., Hersbach, H., Hólm, E.V., Isaksen, L., Kållberg, P., Köhler, M., Matricardi, M., Mcnally, A.P., Monge-Sanz, B.M., Morcrette, J.J., Park, B.K., Peubey, C., de Rosnay, P., Tavolato, C., Thépaut, J.N., Vitart, F., 2011. The ERA-interim reanalysis: configuration and performance of the data assimilation system. Q. J. R. Meteorol. Soc. 137, 553–597. https://doi.org/10.1002/qj.828.

Dereczynski, C., Silva, W.L., Marengo, J., 2013. Detection and projections of climate change in Rio de Janeiro, Brazil. Am. J. Clim. Chang. 2, 25–33. https://doi.org/10.4236/ajcc.2013.21003.

Falagas, M.E., Karageorgopoulos, D.E., Moraitis, L.I., Vouloumanou, E.K., Roussos, N., Peppas, G., Rafailidis, P.I., 2009. Seasonality of mortality: the September phenomenon in Mediterranean countries. CMAJ 181, 484–486. https://doi.org/10.1503/cmaj.090694.

Ferranti, L., Viterbo, P., 2006. The European summer of 2003: sensitivity to soil water initial conditions. J. Clim. 19, 3659–3680. https://doi.org/10.1175/JCLI3810.1.

Filleul, L., Cassadou, S., Médina, S., Fabres, P., Lefranc, A., Eilstein, D., Le Tertre, A., Pascal, L., Chardon, B., Blanchard, M., Declercq, C., Jusot, J.F., Prouvost, H., Ledrans, M., 2006. The relation between temperature, ozone, and mortality in nine French cities during the heat wave of 2003. Environ. Health Perspect. 114, 1344–1347. https://doi.org/10.1289/ehp.8328.

Fischer, E.M., 2014. Autopsy of two mega-heatwaves. Nat. Geosci. https://doi.org/10.1038/ngeo2148.

Fischer, E.M., Seneviratne, S.I., Vidale, P.L., Lüthi, D., Schär, C., 2007. Soil moisture-atmosphere interactions during the 2003 European summer heat wave. J. Clim. (20), 5081–5099 https://doi.org/10.1175/JCLI4288.1.

Frank, N.L., 1970. On the energetics of cold lows. Proceedings Symposium on Tropical Meteorology, Amer. Meteor. Soc EIV 1- EIV 6.

Garcia-Herrera, R., Díaz, J., Trigo, R.M., Luterbacher, J., Fischer, E.M., 2010. A review of the European summer heat wave of 2003. Crit. Rev. Environ. Sci. Technol. 40, 267–306. https://doi.org/10.1080/10643380802238137.

Gasparrini, A., Armstrong, B., 2012. The impact of heat waves on mortality. Epidemiology 22, 68–73. https://doi.org/10.1097/EDE.0b013e3181fdcd99.The.

Gasparrini, A., Guo, Y., Hashizume, M., 2015. Mortality risk attributable to high and low ambient temperature: a multicountry observational study. Lancet 386, 369375. https://doi.org/10.1016/S0140-6736(14)62114-0.

Geirinhas, J.L., Trigo, R.M., Libonati, R., Coelho, C.A.S., Palmeira, A.C., 2017. Climatic and synoptic characterization of heat waves in Brazil. Int. J. Climatol. 38, 1760–1776. https://doi.org/10.1002/joc.5294.
Gouveia, N., Hajat, S., Armstrong, B., 2003. Socioeconomic differentials in the temperature-mortality relationship in São Paulo, Brazil. Int. J. Epidemiol. 32, 390–397. https://doi.org/10.1093/ije/dyg077.
Grimm, A.M., 2003. The El Niño impact on the summer monsoon in Brazil: regional processes versus remote influences. J. Clim. 16, 263–280. https://doi.org/10.1175/1520-0442(2003)016<0263:TENIOT>2.0.CO;2.
Gusso, A., Ducati, J.R., Veronez, M.R., Sommer, V., Junior, Silveira, Da, L.G., 2014. Monitoring heat waves and their impacts on summer crop development in Southern Brazil. Agric. Sci. 05, 353–364. https://doi.org/10.4236/as.2014.54037.
Hajat, S., Armstrong, B.G., Gouveia, N., Wilkinson, P., 2005. Mortality displacement of heat-related deaths: a comparison of Delhi, São Paulo, and London. Epidemiology 16, 613–620. https://doi.org/10.1097/01.ede.0000164559.41092.2a.
Hannart, A., Vera, C., Otto, F.E.L., Cerne, B., 2015. Causal influence of anthropogenic forcings on the Argentinian heat wave of December 2013. Bull. Am. Meteorol. Soc. https://doi.org/10.1175/BAMS-D-15-00137.1.
Herdies, D.L., Da Silva, A., Silva Dias, M.A.F., Ferreira, R.N., 2002. Moisture budget of the bimodal pattern of the summer circulation over South America. J. Geophys. Res. D: Atmos. 107, 1–10. https://doi.org/10.1029/2001JD000997.
Herring, S.C., Hoerling, M.P., Kossin, J.P., Peterson, T.C., Stott, P.A., 2015. Explaining extreme events of 2014 from a climate perspective. Bull. Am. Meteorol. Soc. 96 (12), S1–S172. https://doi.org/10.1175/BAMS-ExplainingExtremeEvents2014.1.
IBGE - Instituto Brasileiro de Geografia e Estatística, 2010. Demographic census. https://censo2010.ibge.gov.br, Accessed date: June 2018.
IPCC, 2012. Managing the risks of extreme events and disasters to advance climate change adaptation. In: Field, C.B., Barros, V.R., Stocker, T.F., Qin, D., Dokken, D.J., Ebi, K.L., Mastrandea, M.D., Mach, K.J., Pçattner, G.-K., Allen, S.K., Tignor, M., Midgley, P.M. (Eds.), A Special Report of Working Groups I and II of the Intergovernmental Panel on Climate Change. Cambridge University Press, Cambridge.
IPCC, 2014. Climate change 2014: impacts, adaptation and vulnerability. Part B: regional aspects. In: Barros, V.R., Field, C.B., Dokken, D.J., Mastrandea, M.D., Mach, K.J., Bilir, T.E., Chatterjee, M., Ebi, K.L., Estrada, Y.O., Genova, R.C., Girma, B., Kissel, E.S., Levy, A.N., MacCracken, S., Mastrandea, P.R., White, L.L. (Eds.), Contribution of Working Group II to the Fifth Assessment Report of the Intergovernmental Panel on Climate Change. Cambridge University, Cambridge.
Irving, D., Simmonds, I., 2016. A new method for identifying the Pacific-South American pattern and its influence on regional climate variability. J. Clim. 29, 6109–6125. https://doi.org/10.1175/JCLI-D-15-0843.1.
Ji, L., Senay, G.B., Verdin, J.P., 2015. Evaluation of the global land data assimilation system (GLDAS) air temperature data products. J. Hydrometeorol. 16, 2463–2480. https://doi.org/10.1175/JHM-D-14-0230.1.
Kim, W., Yeh, S.W., Kim, J.H., Kug, J.S., Kwon, M., 2011. The unique 2009-2010 El Niño event: a fast phase transition of warm pool El Niño to la Niña. Geophys. Res. Lett. 38, 1–5. https://doi.org/10.1029/2011GL048521.
Kousky, V.E., Alonso Gan, M., 1981. Upper tropospheric cyclonic vortices in the tropical South Atlantic. Tellus 33, 538–551. https://doi.org/10.3402/tellusa.v33i6.10775.
Kug, J.S., Jin, F.F., An, S. Il, 2009. Two types of El Niño events: cold tongue El Niño and warm pool El Niño. J. Clim. https://doi.org/10.1175/2008JCLI2624.1.
Lenters, J.D., Cook, K.H., 1997. On the origin of the Bolivian high and related circulation features of the south American climate. J. Atmos. Sci. 54, 656–678. https://doi.org/10.1175/1520-0469(1997)054<0656:OTOOTB>2.0.CO;2.
Lewis, S.L., Brando, P.M., Phillips, O.L., Van Der Heijden, G.M.F., Nepstad, D., 2011. The 2010 Amazon drought. Science 331 (80), 554. https://doi.org/10.1126/science.1200807.
Liebmann, B., Kiladis, G.N., Vera, C.S., Saulo, A.C., Carvalho, L.M.V., 2004. Subseasonal variations of rainfall in South America in the vicinity of the low-level jet east of the Andes and comparison to those in the South Atlantic convergence zone. J. Clim. 17, 3829–3842. https://doi.org/10.1175/1520-0442(2004)017<3829:SVORIS>2.0.CO;2.
Linares, C., Díaz, J., 2008. Impact of high temperatures on hospital admissions: comparative analysis with previous studies about mortality (Madrid). Eur. J. Pub. Health 18, 317–322. https://doi.org/10.1093/eurpub/ckm108.
Lucena, A.J., Rotunno Filho, O.C., França, J.R. de A., Peres, L. de F., Xavier, L.N.R., 2013. Urban climate and clues of heat island events in the metropolitan area of Rio de Janeiro. Theor. Appl. Climatol. 111, 497–511. https://doi.org/10.1007/s00704-012-0668-0.
Marengo, J.A., Camargo, C.C., 2008. Surface air temperature trends in Southern Brazil for 1960-2002. Int. J. Climatol. 28, 893–904. https://doi.org/10.1002/joc.1584.
Marengo, J.A., Espinoza, J.C., 2016. Extreme seasonal droughts and floods in Amazonia: causes, trends and impacts. Int. J. Climatol. 36, 1033–1050. https://doi.org/10.1002/joc.4420.
Marengo, J.A., Soares, W.R., Saulo, C., Nicolini, M., 2004. Climatology of the low-level jet east of the Andes as derived from the NCEP-NCAR reanalyses: characteristics and temporal variability. J. Clim. 17. https://doi.org/10.1175/1520-0442(2004)017<2261:COTLJE>2.0.CO;2 (2291-2280).
Marengo, J.A., Tomasella, J., Alves, L.M., Soares, W.R., Rodriguez, D.A., 2011. The drought of 2010 in the context of historical droughts in the Amazon region. Geophys. Res. Lett. 38, 1–5. https://doi.org/10.1029/2011GL047436.
McMichael, A.J., Wilkinson, P., Kovats, R.S., Pattenden, S., Hajat, S., Armstrong, B., Vajanapoom, N., Niciu, E.M., Mahomed, H., Kingkeow, C., Kosnik, M., O'Neill, M.S., Romieu, I., Ramirez-Aguilar, M., Barreto, M.L., Gouveia, N., Nikiforov, B., 2008. International study of temperature, heat and urban mortality: the "ISOTHURM" project. Int. J. Epidemiol. 37, 1121–1131. https://doi.org/10.1093/ije/dyn086.
Miralles, D.G., Teuling, A.J., Van Heerwaarden, C.C., De Arellano, J.V.G., 2014. Mega-heatwave temperatures due to combined soil desiccation and atmospheric heat accumulation. Nat. Geosci. 7, 345–349. https://doi.org/10.1038/ngeo2141.
Mo, K.C., Paegle, J.N., 2001. The Pacific-South America modes and their downstream effects. Int. J. Climatol. 21, 1211–1229. https://doi.org/10.1002/joc.685.
Muggeo, V.M., Hajat, S., 2009. Modelling the non-linear multiple-lag effects of ambient temperature on mortality in Santiago and Palermo: a constrained segmented distributed lag approach. Occup. Environ. Med. 66, 584–591. https://doi.org/10.1136/oem.2007.038653.
NOAA, 2018. National Centers for Environmental Information, State of the Climate: Global Climate Report for Annual 2017. https://www.ncdc.noaa.gov/sotc/global/201713, Accessed date: 3 April 2018.
Nogueira, P., Paixão, E., 2008. Models for mortality associated with heatwaves: update of the Portuguese heat health warning system. Int. J. Climatol. 28, 545–562. https://doi.org/10.1002/joc.1546.
Nogués-Paegle, J., Mo, K.C., 1997. Alternating wet and dry conditions over South America during summer. Mon. Weather Rev. 125, 279–291. https://doi.org/10.1175/1520-0493(1997)125<0279:AWADCO>2.0.CO;2.
Panisset, J.S., Libonati, R., Gouveia, C.M.P., Machado-Silva, F., França, D.A., França, J.R.A., Peres, L.F., 2018. Contrasting patterns of the extreme drought episodes of 2005, 2010 and 2015 in the Amazon Basin. Int. J. Climatol. 38, 1096–1104. https://doi.org/10.1002/joc.5224.
Peres, L. de F., Lucena, A.J., Rotunno Filho, O.C., França, J.R. de A., 2018. The urban heat island in Rio de Janeiro, Brazil, in the last 30 years using remote sensing data. Int. J. Appl. Earth Obs. Geoinf. 64, 104–116. https://doi.org/10.1016/j.jag.2017.08.012.
Perkins, S.E., 2011. Biases and model agreement in projections of climate extremes over the tropical Pacific. Earth Interact. 15 (24), 1–36. https://doi.org/10.1175/2011EI395.1.
Perkins, S.E., Alexander, L.V., 2013. On the measurement of heat waves. J. Clim. 26, 4500–4517. https://doi.org/10.1175/JCLI-D-12-00383.1.
Qian, W., Wu, K., Leung, J.C.H., 2016. Three-dimensional structure and long-term trend of heat wave events in western Eurasia revealed with an anomaly-based approach. Int. J. Climatol. 36, 4315–4326. https://doi.org/10.1002/joc.4634.
Renom, M., Rusticucci, M., Barreiro, M., 2011. Multidecadal changes in the relationship between extreme temperature events in Uruguay and the general atmospheric circulation. Clim. Dyn. 37, 2471–2480. https://doi.org/10.1007/s00382-010-0986-9.
Renwick, J., Revell, M.J., 1999. Blocking over the South Pacific and Rossby Wave Propagation. Mon. Weather Rev. 127, 2233–2247. https://doi.org/10.1175/1520-0493(1999)127<2233:BOTSPA>2.0.CO;2.
Robine, J.M., Cheung, S.L.K., Le Roy, S., Van Oyen, H., Griffiths, C., Michel, J.P., Herrmann, F.R., 2008. Death toll exceeded 70,000 in Europe during the summer of 2003. C. R. Biol. 331, 171–178. https://doi.org/10.1016/j.crvi.2007.12.001.
Rodrigues, J.A., Libonati, R., Peres, L., Setzer, A., 2018. Mapeamento de áreas queimadas em Unidades de Conservação da região serrana do Rio de Janeiro utilizando o satélite Landsat-8 durante a seca de 2014. Anuário do IGEO 41, 318–327. http://dx.doi.org/10.11137/2018_1_318_327.
Rusticucci, M., 2012. Observed and simulated variability of extreme temperature events over South America. Atmos. Res. 106, 1–17. https://doi.org/10.1016/j.atmosres.2011.11.001.
Rusticucci, M., Kyselý, J., Almeira, G., Lhotka, O., 2016. Long-term variability of heat waves in Argentina and recurrence probability of the severe 2008 heat wave in Buenos Aires. Theor. Appl. Climatol. 124, 679–689. https://doi.org/10.1007/s00704-015-1445-7.
Rusticucci, M., Barrucand, M., Collazo, S., 2017. Temperature extremes in the Argentina central region and their monthly relationship with the mean circulation and ENSO phases. Int. J. Climatol. 37, 3003–3017. https://doi.org/10.1002/joc.4895.
Seneviratne, S.I., Donat, M.G., Mueller, B., Alexander, L.V., 2014. No pause in the increase of hot temperature extremes. Nat. Clim. Chang. 4, 161–163. https://doi.org/10.1038/nclimate2145.
Son, J.Y., Gouveia, N., Bravo, M.A., de Freitas, C.U., Bell, M.L., 2016. The impact of temperature on mortality in a subtropical city: effects of cold, heat, and heat waves in São Paulo, Brazil. Int. J. Biometeorol. 60, 113–121. https://doi.org/10.1007/s00484-015-1009-7.
Sousa, P.M., Trigo, R.M., Barriopedro, D., Soares, P.M.M., Santos, J.A., 2018. European temperature responses to blocking and ridge regional patterns. Clim. Dyn. 50, 457–477. https://doi.org/10.1007/s00382-017-3620-2.
Tomczyk, A.M., 2017. Atmospheric circulation during heat waves in Eastern Europe. Aust. Geogr. 122, 121–146.
Trigo, R.M., Trigo, I.F., DaCamara, C.C., Osborn, T.J., 2004. Climate impact of the European winter blocking episodes from the NCEP/NCAR reanalyses. Clim. Dyn. 23, 17–28. https://doi.org/10.1007/s00382-004-0410-4.
Trigo, R.M., García-Herrera, R., Díaz, J., Trigo, I.F., Valente, M.A., 2005. How exceptional was the early August 2003 heatwave in France? Geophys. Res. Lett. 32, L10701. https://doi.org/10.1029/2005GL022410.
Trigo, R.M., Ramos, A.M., Nogueira, P.J., Santos, F.D., Garcia-Herrera, R., Gouveia, C., Santo, F.E., 2009. Evaluating the impact of extreme temperature based indices in the 2003 heatwave excessive mortality in Portugal. Environ. Sci. Pol. 12, 844–854. https://doi.org/10.1016/j.envsci.2009.07.007.
Vandentorren, S., Bretin, P., Zeghnoun, A., Mandereau-Bruno, L., Croisier, A., Cochet, C., Ribéron, J., Siberan, I., Declercq, B., Ledrans, M., 2006. August 2003 heat wave in France: risk factors for death of elderly people living at home. Eur. J. Pub. Health 16, 583–591. https://doi.org/10.1093/eurpub/ckl063.
Wright, J.S., Fueglistaler, S., 2013. Large differences in reanalyses of diabatic heating in the tropical upper troposphere and lower stratosphere. Atmos. Chem. Phys. 13, 9565–9576. https://doi.org/10.5194/acp-13-9565-2013.
Yu, W., Vaneckova, P., Mengersen, K., Pan, X., Tong, S., 2010. Is the association between temperature and mortality modified by age, gender and socio-economic status? Sci. Total Environ. 408, 3513–3518. https://doi.org/10.1016/j.scitotenv.2010.04.058.